Sumatra2004.html (Y. Yagi), and www.geop.itu.edu.tr/%7Etaymaz/sumatra (T. Taymaz, O. Tan, S. Yolsal).
27. S. Das, B. V. Kostrov, *Phys. Earth Planet. Inter.* **85**, 293 (1994).
28. H. K. Thio, R. W. Graves, P. G. Somerville, T. Sato, T. Ishii, *J. Geophys. Res.* **109**, 10.1029/2002JB002381 (2004).
29. C. Ji, D. J. Wald, D. V. Helmberger, *Bull. Seismol. Soc. Am.* **92**, 1192 (2002).
30. C. Ji, D. J. Wald, D. V. Helmberger, *Bull. Seismol. Soc. Am.* **92**, 1208 (2002).
31. C. Ji, D. V. Helmberger, D. J. Wald, K.-F. Ma, *J. Geophys. Res.* **108**, 10.1029/2002JB001764 (2003).
32. K. Sieh, *Nature* **434**, 573 (2005).
33. G. Ekström, J. Tromp, E. W. F. Larson, *J. Geophys. Res.* **102**, 8137 (1997).
34. J. Park *et al.*, *Science* **308**, 1139 (2005).
35. O. Gudmundsson, M. A. Sambridge, *J. Geophys. Res.* **103**, 7121 (1998).
36. R. A. Kerr, *Science* **308**, 341 (2005).
37. Information about the Center for Earth Science Studies Seismology Research Group is available online at www.seires.net/content/view/123/52/.
38. We acknowledge the efforts of those associated with the collection of data made freely available through the Federation of Digital Broadband Seismographic Networks. Seismic waveform data were obtained from the Incorporated Research Institutions for Seismology (IRIS) Data Management System. This work was supported in part by NSF contracts EAR-0125595 and EAR-0337491, USGS contract 04HQGR0038, and the California Institute of Technology Tectonics Observatory. S.N. was supported in part by the Outstanding Young Scientists Program of the National Science Foundation of China (40425005).

Supporting Online Material
www.sciencemag.org/cgi/content/full/308/5725/1133/DC1
Materials and Methods
Figs. S1 to S13
Table S1
Movies S1 to S3

14 March 2005; accepted 27 April 2005
10.1126/science.1112260

RESEARCH ARTICLE

Earth's Free Oscillations Excited by the 26 December 2004 Sumatra-Andaman Earthquake

Jeffrey Park,[1] Teh-Ru Alex Song,[2] Jeroen Tromp,[2] Emile Okal,[3] Seth Stein,[3] Genevieve Roult,[4] Eric Clevede,[4] Gabi Laske,[5] Hiroo Kanamori,[2] Peter Davis,[5] Jon Berger,[5] Carla Braitenberg,[6] Michel Van Camp,[7] Xiang'e Lei,[8] Heping Sun,[8] Houze Xu,[8] Severine Rosat[9]

At periods greater than 1000 seconds, Earth's seismic free oscillations have anomalously large amplitude when referenced to the Harvard Centroid Moment Tensor fault mechanism, which is estimated from 300- to 500-second surface waves. By using more realistic rupture models on a steeper fault derived from seismic body and surface waves, we approximated free oscillation amplitudes with a seismic moment (6.5×10^{22} Newton·meters) that corresponds to a moment magnitude of 9.15. With a rupture duration of 600 seconds, the fault-rupture models represent seismic observations adequately but underpredict geodetic displacements that argue for slow fault motion beneath the Nicobar and Andaman islands.

The 26 December 2004 Sumatra-Andaman earthquake delivered a blow to our planet (*1*, *2*), exciting a plethora of vibrational free oscillations that, at periods $T > 1000$ s, remained observable for weeks in broadband seismic data from global networks. The frequencies and decay rates of Earth's free oscillations offer strong constraints (*3*–*5*) on our planet's interior composition, mineralogy, and dynamics (*6*–*15*), so analysis of long-period seismic data from this event should offer new perspectives on Earth structure. In this report, we discuss how seismic free oscillations also provide information on the size and duration of this earthquake.

[1]Department of Geology and Geophysics, Yale University, Post Office Box 208109, New Haven, CT 06520–8109, USA. [2]Seismological Laboratory, California Institute of Technology, MS 252–21, Pasadena, CA 91125, USA. [3]Department of Geological Sciences, 1850 Campus Drive, Evanston, IL 60208–2150, USA. [4]Departement de Sismologie, Institut de Physique du Globe de Paris (IPGP), 4 Place Jussieu, 75252 Paris Cedex 05, France. [5]Scripps Institution of Oceanography, University of California, San Diego, La Jolla, CA 92093–0225, USA. [6]Dipartimento di Scienze della Terra, Universita' di Trieste, Via Weiss 1, 34100 Trieste, Italy. [7]Royal Observatory of Belgium, Avenue Circulaire 3, B–1180 Bruxelles, Belgium. [8]Institute of Geodesy and Geophysics, Chinese Academy of Sciences, 174 Xudong Road, Wuhan 430077, China. [9]National Astronomical Observatory of Japan, 2–12 Hoshigaoka, Mizusawa, Iwate 023–0861, Japan.

Because Earth is roughly spherical, the geographical patterns of its free vibrational modes can be expressed in terms of the spherical harmonics, $Y_{lm}(\theta,\phi)$, and their vector gradients, where l is the angular degree, m is the azimuthal order, θ is colatitude, and ϕ is longitude. On a simple spherical planet (*16*), the free oscillations follow either a spheroidal (S) or toroidal (T) vibrational pattern and have spectroscopic notation ${}_nS_{lm}$ and ${}_nT_{lm}$, $m = -l,\ldots,l$, where n is the radial overtone number (Fig. 1). For a spherical reference model, all $2l + 1$ vibrations of ${}_nS_{lm}$ or ${}_nT_{lm}$ have identical frequency. On the real Earth, departures from the symmetries of a spherical reference model cause its free oscillations to couple, hybridize, and suffer fine-scale splitting of their vibrational frequencies (*17*–*20*). Frequency splitting of free oscillations with periods $T > 1000$ s is caused mainly by Earth's rotation, similar to Zeeman splitting of electron energies in an external magnetic field (*21*, *22*).

Earth's free oscillations were first reported after Fourier analysis of hand-digitized analog seismic records of the megathrust earthquakes of the middle 20th century (*23*–*26*), particularly the 22 May 1960 Chilean earthquake ($M_w = 9.5$). These huge events saturated most seismometers of the time, rendering many hours of data unusable. Frequency estimates from smaller, deeper earthquakes, more amenable to hand-digitization and Fourier analysis, led to accurate spherical-reference models for our planet's interior (*6*). Detailed study of free-oscillation attenuation, frequency splitting, and modal coupling was made feasible by digital recording (*7*, *8*, *27*, *28*) and by the advent of the Federation of Digital Seismic Networks (FDSN) with high-dynamic range induction-feedback sensors capable of recording faithfully the seismic waves from great earthquakes (*29*, *30*).

Broadband seismographic data. The 2004 Sumatra-Andaman earthquake tested broadband seismographic technology on a global scale. Peak ground motions exceeded 1 cm at all locations on Earth's solid surface (*31*). In one portion of the FDSN, 88% of the 125 stations of the Global Seismographic Network (GSN), operated by the U.S. Geological Survey and Project IDA of the University of California, San Diego (*32*, *33*), recorded data without interruption or distortion (*34*). Stations of the Geoscope network (*35*, *36*) had similar success.

In all, data records from more than 400 FDSN stations had sufficient quality to observe Earth's free oscillations with unprecedented signal-to-noise ratios. A broad distribution of stations facilitates the use of spherical harmonic-weighted stacks of data spectra to isolate individual Earth vibrations (fig. S2). The recent installation of a broadband seismometer in the South Pole quiet zone provides natural isolation of the $m = 0$ singlets of long-period modes (Fig. 2). Free oscillations can also be sought in complementary observations (Fig. 3) from strainmeters and tiltmeters (*37*–*40*), from superconducting gravimeters (*41*–*43*), and from continuously recording global positioning system (GPS) receivers (*44*, *45*). Superconducting gravimeter data offers an important

calibration for seismometer data at periods $T >$ 1000 s (*46*). The amplitude of the "breathing mode" ${}_0S_0$ is geographically constant to high accuracy; station-by-station comparisons of its amplitude in data from the IDA network suggest that a substantial minority of seismometers suffer 5 to 10% deviations from their nominal responses (*34*).

The largest earthquakes offer the most penetrating and long-lasting seismic probes of Earth's deep interior, revealing behavior predicted by theory but only rarely observed above ground noise. The coupling between spheroidal and toroidal modes associated with Earth's Coriolis force causes them to form hybrid vibrational patterns. The hybridized toroidal modes are predicted to acquire a vertical vibrational component, a feature nominally restricted to spheroidal modes. Although this behavior is readily observable for mode pairs ${}_0S_l - {}_0T_{l+1}$ in the 300- to 500-s period range that are close in frequency (*27*, *28*), at frequencies below 1 mHz the coupling is weaker and was not observed with seismometers before the 2004 Sumatra-Andaman earthquake (*47*) (Fig. 1 and fig. S3).

The geometry of low-degree modes allows us to constrain the long-period centroid of the earthquake (*8*, *23*). For a centroid at the equator, excitation of the $m = \pm 1$ vibrations of the mode ${}_0S_2$ would be zero for an earthquake on the east-dipping Sumatra-Andaman thrust fault. The amplitude of the $m = -1, +1$ vibrations of ${}_0S_2$ relative to the $m = -2$, 0, and $+2$ vibration indicates how far northward the Sumatra-Andaman earthquake ruptured (Fig. 4). The event hypocenter and Centroid Moment Tensor (CMT) location lie at 3.2°N and 3.1°N, respectively, displaced east-west by nearly 200 km. The relative excitation of the $m = \pm 1$ vibrational modes of ${}_0S_2$ is significantly underpredicted by this location centroid. Better agreement is obtained for a seismic source centroid closer to 7.5°N, suggesting a source process that extends into the northern half of the aftershock zone.

Earthquake size and duration. Since the late 1970s, seismologists have estimated magnitude M_w for large earthquakes in terms of the seismic moment M_o (*48*). As a measure of the average displacement integrated over the ruptured fault zone, M_o is associated with its behavior at zero frequency. It is therefore logical to estimate M_o from the amplitudes of the gravest Earth free oscillations, such as the modes ${}_0S_2$, ${}_0S_3$, ${}_0S_4$, ${}_0S_0$, and ${}_1S_0$. For nearly all earthquakes, these modes are excited too weakly for direct observation, but the Sumatra-Andaman event was different. The "football mode" ${}_0S_2$, the free oscillation with the longest observed period (53.7 min), is expressed strongly in vertical-component spectra computed from a large proportion of individual stations, as are many of the shorter-period modes. The amplitudes of several spheroidal free oscillations with periods $T >$ 1000 s were a factor of 1.25 to 2.6 larger than those predicted by the Harvard CMT source (*1*–*3*), reaching a maximum for the mode ${}_0S_2$ (Figs. 4 and 5). If this amplitude is related to fault motion with the same geometry as the CMT solution, i.e., thrusting on a shallow-dipping fault (8° dip), the estimated earthquake magnitude M_w increases from 9.0 to 9.3.

Source spectral amplitude is larger at long periods for earthquakes with long time durations. If seismic rupture progresses at a constant rate for a finite duration τ from a sharp onset to an equally abrupt termination, the source spectrum $M(f)$ equals $M_o(\sin \pi f\tau)/(\pi f\tau)$ as a function of cycle frequency f (*49*). The logarithm of $M(f)$ exhibits a low-frequency plateau that transitions to a power-law slope at a corner frequency $f_c = (\pi\tau)^{-1}$. Figure 5 graphs the source spectra implied by several spheroidal modes against $M(f)$ source spectra for constant-rupture durations τ = 800 s and τ = 320 s. Modal amplitudes do not follow the predictions of a constant-rate source spectrum, suggesting a variable rupture-propagation rate. For example, the rupture of two large fault

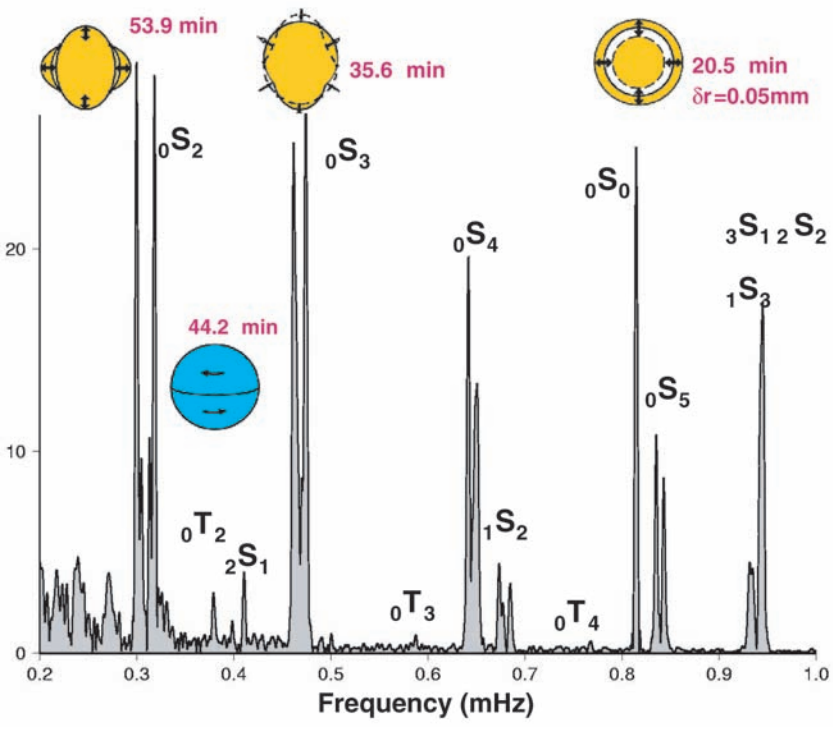

Fig. 1. Schematic of the motion of free oscillations ${}_0S_2$, ${}_0T_2$, ${}_0S_3$, and ${}_0S_0$ superimposed on a spectrum computed from 240 hours of vertical seismic motions recorded at the CAN (Canberra, Australia) station of the Geoscope Network. For comparison, fig. S1 plots the acceleration spectrum from the superconducting gravimeter collocated with CAN.

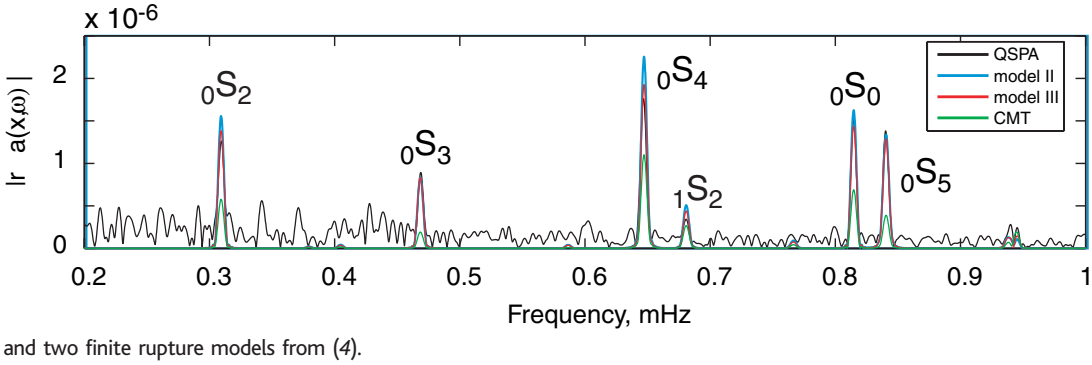

Fig. 2. Free-oscillation spectra for GSN station QSPA, whose sensor lies within an ice borehole in the quiet sector of the South Pole station. Only $m = 0$ free oscillations are nonzero at Earth's poles, leading to sharply defined single resonance peaks for modes ${}_nS_l$ and ${}_nT_l$ with period $T >$ 1000 s. A vertical-motion data series of 106 hours was analyzed. Predicted spectra are plotted with colored lines from Harvard CMT mechanism and two finite rupture models from (*4*).

segments with different orientations, onset times, and durations would cause spectral interference at long periods, as would a more complex rupture history. Such complexity aside, the trend of modal amplitudes is consistent with a rupture duration $\tau \leq 800$ s.

The initial phase of ${}_0S_0$ relative to the earthquake onset supports the inference of long-source duration τ. The initial phase of a free oscillation of period T aligns with the time centroid of the rupture process if the rupture duration is relatively small, i.e., $\tau \ll T$. Phase cancellation dampens the modal excitation if $\tau \geq T/2$, and the relation of modal initial phases with the source time centroid becomes complicated. We estimate the initial phase of ${}_0S_0$ to average 65° to 66° in the GSN and to average 61° over nine records from the Geoscope network (fig. S4). The initial displacement of ${}_0S_0$ is positive (0° phase), so this suggests a time centroid delayed 205 to 225 s relative to the earthquake onset. Rupture duration τ was between 400 and 450 s if the rupture rate were constant. The initial phase of ${}_1S_0$ is 115.7° averaged for nine Geoscope stations, consistent with a time centroid of 197 s. A variable rupture rate will cause scatter in time centroids estimated from different modes.

Free-oscillation observations constrain the Sumatra-Andaman earthquake source, but the constant-rupture model is too simple. A complex earthquake process is suggested by a number of observations, e.g., large bursts of high-frequency seismic radiation occurred in the first 200 s of rupture (*4*, *50*); aftershock locations spanned a 1300-km segment of plate margin (*5*), but in the northern 400 km of the zone the aftershocks commenced some 85 min after rupture onset (*51*); substantial surface-wave directivity at periods approaching 1000 s (*4*); the dip of the Sumatra-Andaman megathrust in its northern half tended to exceed the 8° dip of the Harvard CMT source mechanism (*5*); back-arc spreading in the Andaman Sea may have promoted the expression of strike-

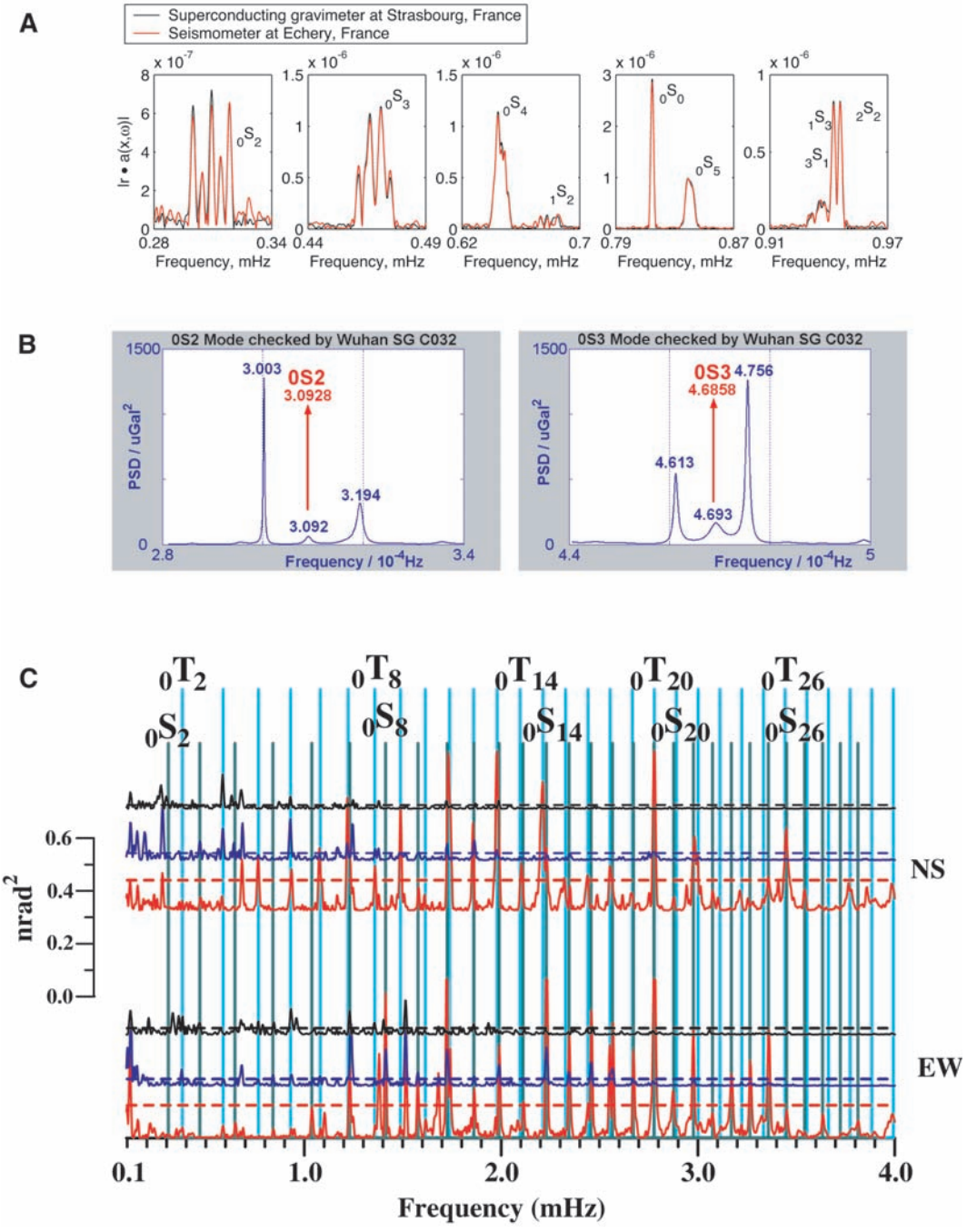

Fig. 3. Spectrum comparison for the 26 December 2004 Sumatra-Andaman earthquake. (**A**) Superconducting gravimeter (Strasbourg, France) and nearby vertical-component seismic data (Echery, France) have almost identical spectra. The multiple spectral peaks, e.g., of ${}_0S_2$, are caused by splitting associated with Earth rotation. A Hann taper has been applied to the 230-hours time series from both instruments before discrete Fourier transformation: (**B**) Burg-method spectrum estimates of data from the C032 superconducting gravimeter (SG) at Wuhan station, People's Republic of China, and (**C**) Blackman-Tukey-tapered spectral estimates of horizontal-component data from the Grotta Gigante pendulum tiltmeter, computed on three sliding time windows of 24 hours each, shifted by 12 hours. The red, blue, and black lines pertain to the windows starting at days 361.25, 361.75, and 362.25 of 2004, respectively. North-south motion is shown in top three traces; east-west motion is shown in the bottom traces. The broken line indicates the 95% confidence level at which a spectral peak is significant.

slip motion as the rupture progressed north (*5*); modeling suggests that the northern third of the fault zone contributed little to the observed tsunami (*5*). Many factors suggest that fault motion was larger and faster in the south of the fault zone, where rupture began, and was smaller and slower in the north.

Modeling the rupture. Drawing on inferences made from these data, we consider here two finite-rupture models based on body and surface waves [models II and III of (*4*)] in which rupture has longer duration (600 s versus 300 s), longer length (1300 km versus ~400 km), and larger moment (6.5×10^{22} N·m versus 4.0×10^{22} N·m) than that inferred from the CMT solution (Fig. 6). Both models prescribe a spatially varying fault geometry that is, on average, steeper than the CMT solution. A steeper fault is more efficient at exciting the long-period modes, and therefore the finite rupture models can greatly improve the match between predicted and observed modal amplitudes (*52*–*56*) with a far smaller M_o than inferred by (*3*). A transition to oblique thrust motion in the Andaman islands region improves the fit to long-period toroidal modes. Model III, which prescribes a peak rate of rupture propagation somewhat earlier than model II, is slightly more successful at predicting the absolute value of modal vertical-component spectral peaks, typically with an average misfit pf less than 10%, depending on the mode (Figs. 2, 7, and 8 and table S1).

Despite the rough success of a single seismic rupture model across the entire seismic spectrum, geodetic evidence for a slow component of Sumatra-Andaman displacement cannot be dismissed. A fault slip of ~1 hour in duration, as suggested by tsunami modeling for the Nicobar-Andaman fault segment (*5*), would excite seismic free oscillations inefficiently because of phase cancellation. Its signature would be expressed as a complex pattern of modal amplitude and phase anomalies. Modal spectra for the 2004 Sumatra Andaman earthquake are more difficult to predict with simple parameterized rupture models than modal spectra from the 28 March 2005 northern Sumatra earthquake ($M_w = 8.6$), despite higher signal-to-noise ratios in the larger event (Fig. 8). If amplitude and phase misfits leave unexplained 10% or more of the long-period free-oscillation amplitudes of the 2004 event, slow fault motion equivalent to at least $M_w = 8.4$ would be possible, a geophysical event larger than any earthquake between 1965 and 2001.

For both Sumatra earthquakes, modal amplitude and phase anomalies will constrain any additional long-term slip. In this context, the calibration and long-term resilience of global seismographic networks is paramount. A future megathrust earthquake ($M_w \geq 9.0$) is inevitable somewhere along Earth's plate boundaries but may occur after today's seismometers have begun to age and perhaps fail. The broadband vault seismometer most suitable for today's global seismographic networks, the Streckeisen STS-1 (*57*), is no longer manufactured. It is important for the international seismological community to consider designing the next-generation broadband seismic sensor.

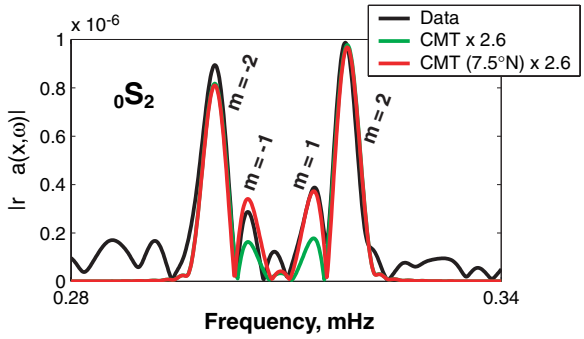

Fig. 4. Observed and predicted $_0S_2$ spectra at SCSN station OSI (Osito Adit, California). Black curve is data; red, prediction for the Harvard CMT mechanism and location but with scalar moment increased by a factor of 2.6. Note how the $m = 1$ and $m = -1$ singlets are too small, indicating that the CMT centroid is too close to the equator. Green curve is prediction for the CMT moment, increased by a factor of 2.6 and shifted to a centroid location at 7.5°N. This shift improves the fit to the $m = 1$ and $m = -1$ singlets. A Hann taper has been applied to the 144-hour time series.

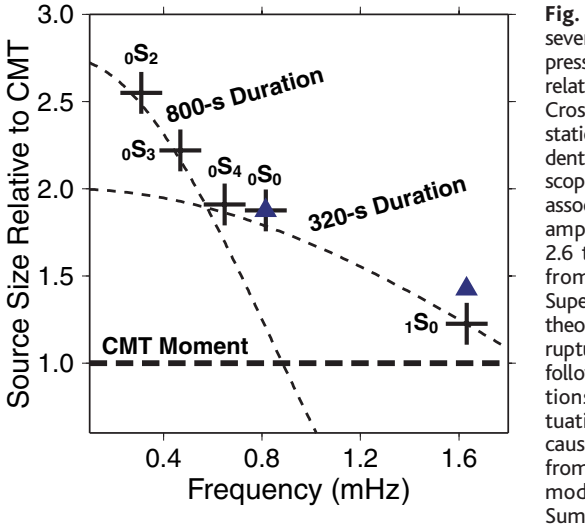

Fig. 5. The measured amplitudes of several long-period free oscillations, expressed in terms of their amplitude excess relative to the Harvard CMT solution. Crosses indicate estimates from GSN stations; triangles are estimated independently with the use of data from Geoscope stations. The largest amplification is associated with the mode $_0S_2$, whose amplitude seems to require roughly 2.6 times the CMT moment estimated from 300- to 500-s surface waves. Superimposed on the measurements are theoretical source spectra for constant-rupture sources of duration τ, which follow $\sin(\pi f\tau)/(\pi f\tau)$ dependence. Deviations in source geometry and fluctuations in rupture rate would cause cause the source spectrum to depart from this simple model. Nevertheless, modal excitation suggests that the Sumatra-Andaman earthquake involved fault slip on more than one time scale.

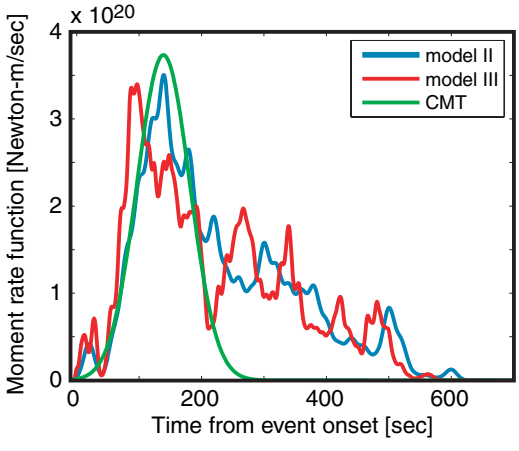

Fig. 6. Moment-rate functions (MRFs) for the 26 December Sumatra-Andaman earthquake. The MRF associated with the Harvard CMT is given by the green line, the MRF of finite-fault inversion II of (*4*) is denoted by the blue line, and the MRF of finite-fault inversion III of (*4*) is denoted by the red line.

References and Notes

1. G. Ekström, A. M. Dziewonski, N. N. Maternovskaya, M. Nettles, *Phys. Earth Planet. Inter.* **148**, 327 (2005).
2. Harvard CMT solutions can be accessed at www.seismology.harvard.edu/CMTsearch.html.
3. S. Stein, E. Okal, *Nature* **434**, 581 (2005).
4. C. J. Ammon *et al.*, *Science* **308**, 1133 (2005).
5. T. Lay *et al.*, *Science* **308**, 1127 (2005).
6. F. Gilbert, A. M. Dziewonski, *Philos. Trans. R. Soc. London Ser. A* **278**, 187 (1975).
7. R. Buland, J. Berger, F. Gilbert, *Nature* **277**, 358 (1979).
8. R. J. Geller, S. Stein, *Bull. Seismol. Soc. Am.* **69**, 1671 (1979).
9. J. P. Davis, *Geophys. Res. Lett.* **12**, 141 (1985).
10. D. Giardini, X. Li, J. H. Woodhouse, *Nature* **325**, 405 (1987).
11. M. Ritzwoller, G. Masters, F. Gilbert, *J. Geophys. Res.* **93**, 6369 (1988).
12. R. Widmer, G. Masters, F. Gilbert, *Geophys. J. Int.* **104**, 541 (1991).
13. G. Laske, G. Masters, *Nature* **402**, 66 (1999).

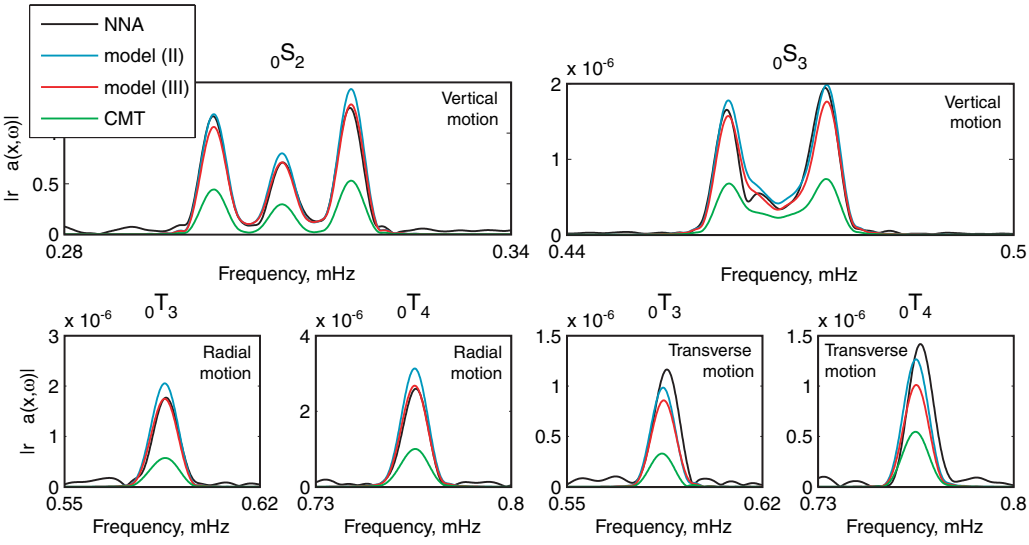

Fig. 7. Comparison of data (NNA, at Nana, Peru) and synthetics from various models. Low-order spheroidal modes $_0S_2$, $_0S_3$ at vertical component and toroidal modes $_0T_3$, $_0T_4$ at horizontal component are shown (**top**). A Hann taper is applied to 144-hours time series of vertical motion before discrete Fourier transformation. Similar tapering was performed on 44-hour time series of radial and transverse horizontal motion before discrete Fourier transformation.

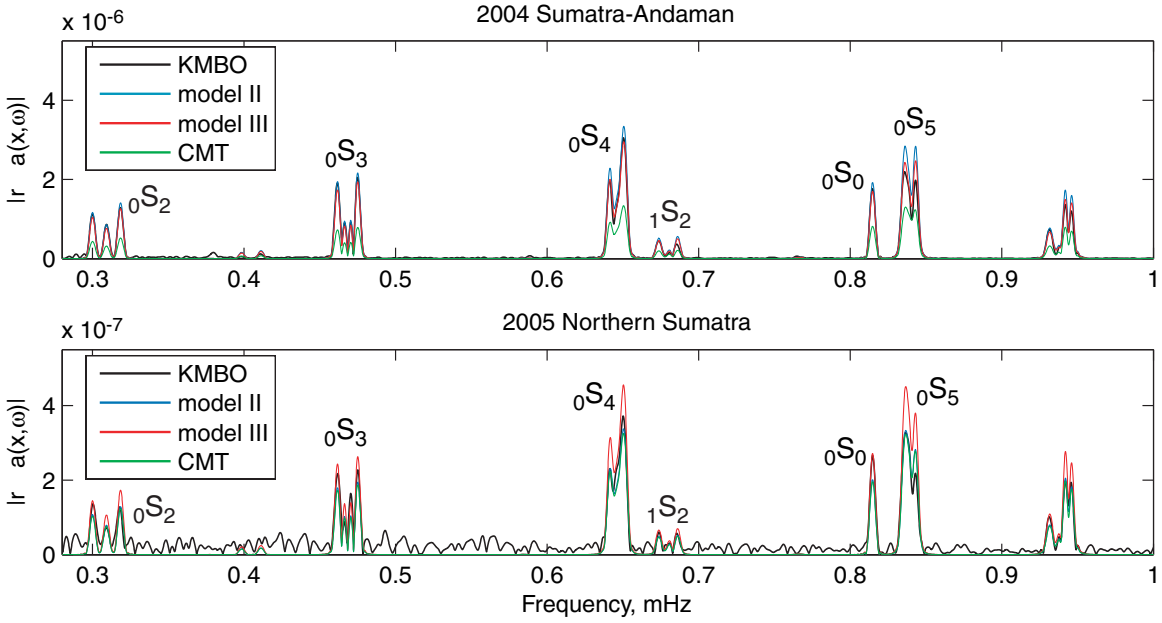

Fig. 8. Spectrum comparison for the 26 December 2004 Sumatra-Andaman and 28 March 2005 Northern Sumatra earthquakes using 127-hour records of vertical motion recorded at station KMBO (Kilima Mbogo, Kenya). Spectral predictions of the Harvard CMT solutions are graphed as well as spectra predicted from finite-rupture models from (*4*). Note the greater success of the CMT solution for the 2005 event, consistent with a smaller less complex rupture process.

14. M. Ishii, J. Tromp, *Science* **285**, 1231 (1999).
15. G. Roult, E. Clevede, *Phys. Earth Planet. Inter.* **121**, 1 (2000).
16. F. A. Dahlen, J. Tromp, *Theoretical Global Seismology* (Princeton Univ. Press, Princeton, NJ, 1998). A spherical reference model describes a nonrotating planet whose stress-strain relation is elastic and either is isotropic or else exhibits anisotropy with a radial axis of symmetry.
17. J. H. Woodhouse, *Geophys. J. R. Astron. Soc.* **61**, 261 (1980).
18. F. A. Dahlen, *Geophys. J. R. Astron. Soc.* **66**, 1 (1981).
19. J. Park, F. Gilbert, *J. Geophys. Res.* **91**, 7241 (1986).
20. P. Lognonne, B. Romanowicz, *Geophys. J. Int.* **102**, 365 (1990).
21. G. Backus, F. Gilbert, *Proc. Natl. Acad. Sci. U.S.A.* **47**, 362 (1961).
22. F. A. Dahlen, R. V. Sailor, *Geophys. J. R. Astron. Soc* **58**, 609 (1979).
23. H. V. Benioff, F. Press, S. W. Smith, *J. Geophys. Res.* **66**, 605 (1961).
24. N. F. Ness, J. C. Harrison, L. B. Slichter, *J. Geophys. Res.* **66**, 621 (1961).
25. L. E. Alsop, G. H. Sutton, M. Ewing, *J. Geophys. Res.* **66**, 631 (1961).
26. S. W. Smith, *J. Geophys. Res.* **71**, 1183 (1966).
27. G. Masters, J. Park, F. Gilbert, *J. Geophys. Res.* **88**, 10285 (1983).
28. W. Zürn, G. Laske, R. Widmer, F. Gilbert, *Geophys. J. Int.* **143**, 113 (2000).
29. B. A. Romanowicz, D. Giardini, *Science* **293**, 2000 (2001).
30. More information is available online at www.fdsn.org.
31. J. Park *et al.*, *Eos* **86**, 57 (2005).
32. R. Butler *et al.*, *Eos* **85**, 225 (2004).
33. More information is available online at www.iris.edu.
34. J. Park *et al.*, *Seism. Res. Lett.* **76**, 329 (2005).
35. G. Roult *et al.*, *Phys. Earth Planet. Int.* **113**, 25 (1999).
36. More information is available online at http://geoscope.ipgp.jussieu.fr.
37. N. R. Goulty, G. C. P. King, A. J. Wallard, *Nature* **246**, 470 (1973).
38. B. A. Bolt, R. G. Currie, *Geophys. J. R. Astron. Soc.* **40**, 107 (1975).
39. M. Zadro, C. Braitenberg, *Earth Sci. Rev.* **47**, 151 (1999).
40. The Grotta Gigante pendulum tiltmeter recorded both the 1960 Chile and the 2004 Sumatra-Andaman earthquakes.
41. M. Van Camp, *Phys. Earth Planet. Inter.* **116**, 81 (1999).
42. K. Nawa *et al.*, *Phys. Earth Planet. Inter.* **120**, 289 (2000).
43. X. Lei, H. Xu, H. Sun, *Chin. Sci. Bull.* **47**, 1573 (2002).
44. K. M. Larson, P. Bodin, J. Gomberg, *Science* **300**, 1421 (2003); published online 15 May 2003 (10.1126/science.1084531).
45. Free oscillations may be resolvable if GPS data from a global network are stacked and corrections for second-order ionospheric effects remove biases that are spatially broad; see (*58*).
46. To calibrate gravimeter and seismometer spectra, the free-oscillation spectral peaks must be corrected for the motion-induced gravitational forces on the seismic sensor (*16*). The breathing mode $_0S_0$ involves only motion parallel to Earth's radius, and the free-air correction to local gravity magnifies its apparent motion by 12%. For data from the Sumatra-Andaman earthquake, an apparent initial amplitude of 55 μm for $_0S_0$ shrinks to 49 μm after this correction. Similar corrections must be made for all modal amplitudes at frequencies f = 1000 s), including corrections for motion-induced accelerations associated with tilt and redistribution of Earth's mass. For instance, the true vertical motion of the football mode $_0S_2$ is 81.2% that computed from the seismometer response alone.
47. The instrumental self-noise of the broadband seismometers used in global seismic networks increases at low frequencies. Earth's gravest free oscillations have therefore been studied primarily with superconducting gravimeter data, not seismometer records, after correction for fluctuations in atmospheric pressure (*28, 59–61*). The signal-to-noise ratio for seismometer records of the 23 June 2001 Peru event (M_w = 8.4) was not high enough to allow the observation of hybridized toroidal modes on the vertical

seismic components, but they are evident for the 2004 Sumatra-Andaman earthquake.
48. T. C. Hanks, H. Kanamori, *J. Geophys. Res.* **84**, 2348 (1979).
49. S. Stein, M. Wysession, *An Introduction to Seismology, Earthquakes, and Earth Structure* (Blackwell Scientific, Malden, MA, 2003).
50. M. Ishii, P. Shearer, H. Houston, J. Vidale, *Nature,* in press.
51. R. Bilham, E. R. Engdahl, N. Feldl, S. P. Satyabala, *Seism. Res. Lett.,* in press.
52. Synthetics are computed according to normal-mode perturbation theory (*16*). Perturbations from a spherical nonrotating Earth model, such as rotation, ellipticity, and lateral heterogeneity are included. We adopt mantle model S20RTS (*53*) and crustal model crust2.0 (*54*) to account for lateral heterogeneity. The latest estimates of spheroidal and toroidal eigenfrequencies and quality factors are used in the calculation (*55*). Modal splitting and coupling due to rotation, ellipticity, and lateral heterogeneity are accounted for on the basis of a group coupling scheme using 36 subgroups of 117 modes below 3 mHz (*56*).
53. J. Ritsema, H. J. van Heijst, *Sci. Prog. (New Haven)* **83**, 243 (2000).
54. C. Bassin, G. Laske, G. Masters, *Eos* **81** (Fall Meeting Suppl.), F897 (abstr. S21A-03) (2000).
55. The Reference Earth Model Web site is at http://mahi.ucsd.edu/Gabi/rem.html.
56. A. Duess, J. Woodhouse, *Geophys. J. Int.* **146**, 833 (2001).
57. R. Pillet, N. Florsch, J. Hinderer, D. Rouland, *Phys. Earth Planet. Inter.* **84**, 161 (1994).
58. S. Kedar, G. A. Hajj, B. D. Wilson, M. B. Heflin, *Geophys. Res. Letts.*, *30*, 1829, doi:10.1029/2003GL017639 (2003).
59. W. Zürn, R. Widmer, *Geophys. Res. Lett.* **22**, 3537 (1995).
60. M. Van Camp, *Phys. Earth Planet. Inter.* **116**, 81 (2000).
61. S. Rosat, J. Hinderer, L. Rivera, *Geophys. Res. Let.*, *30*, 2111, doi:10.1029/2003GL018304 (2003).

62. This work was supported in part by NSF. Seismic waveform data from the Global Seismographic Network (funded by NSF and U.S. Geological Survey) were obtained from the Incorporated Research Institutions for Seismology (IRIS) Data Management System. Seismic waveform data was also obtained from the Geoscope Program (IPGP France) and the Southern California Earthquake Center.

Supporting Online Material
www.sciencemag.org/cgi/content/full/308/5725/1139/DC1
SOM Text
Figs. S1 to S5
Table S1

15 March 2005; accepted 29 April 2005
10.1126/science.1112305

REPORT

Periodically Triggered Seismicity at Mount Wrangell, Alaska, After the Sumatra Earthquake

Michael West,* John J. Sánchez, Stephen R. McNutt

As surface waves from the 26 December 2004 earthquake in Sumatra swept across Alaska, they triggered an 11-minute swarm of 14 local earthquakes near Mount Wrangell, almost 11,000 kilometers away. Earthquakes occurred at intervals of 20 to 30 seconds, in phase with the largest positive vertical ground displacements during the Rayleigh surface waves. We were able to observe this correlation because of the combination of unusually long surface waves and seismic stations near the local earthquakes. This phase of Rayleigh wave motion was dominated by horizontal extensional stresses reaching 25 kilopascals. These observations imply that local events were triggered by simple shear failure on normal faults.

After the great earthquake in Sumatra (*1*), local earthquakes spaced evenly in time occurred at Mount Wrangell, one of the world's largest andesite shield volcanoes. Located in south-central Alaska, Mount Wrangell anchors the eastern end of the Aleutian-Alaska chain of arc volcanoes (Fig. 1). Fumaroles, frequent seismicity, and historical steam plumes attest to Wrangell's active geothermal system (*2*). Because of its volcanic and seismic activity, a network of seismometers is jointly operated in the Wrangell area by the Alaska Volcano Observatory and the Alaska Earthquake Information Center. Surface waves from the moment magnitude (M_w) 9.0 Sumatra earthquake on 26 December 2004 propagated across the regional network and produced vertical trough-to-peak ground displacements of 1.5 cm. A swarm of 14 earthquakes near Mount Wrangell occurred during the passage of the Rayleigh waves (fig. S1), about 1 hour after the initial rupture in Indonesia (Fig. 2).

Six of the local events were large enough to be located. All of these were within 10 km of the summit caldera. The local signals were strongest near the summit at station WANC, suggesting even tighter clustering. Determination of precise locations and focal mechanisms was inhibited by the emergent waveforms and the modest four-station local network. With one exception, located events occurred at depths of 2 km or less. Magnitudes ranged up to local magnitude 1.9. The variation in waveforms and amplitudes, and the scatter in event locations, indicate that the triggered events were not coming from a single source but instead were dispersed around the summit. Some of the waveforms may be composites of more than one simultaneous event. Although 90% of the routinely located seismicity at Wrangell is of the long-period type (*3*), the events in the triggered cluster appear to have been high-frequency tectonic events (except for event 3, Fig. 2B).

Small earthquakes are common at Wrangell. A comparison to the two days before and after the Sumatra earthquake, however, shows a less than 1% probability of six randomly occurring events of any type in any 10-min window. This probability is further decreased by the requirement of magnitudes up to 1.9; high-frequency tectonic origin; even spacing between events; and coincident timing with teleseismic Rayleigh wave ground motion. Although these

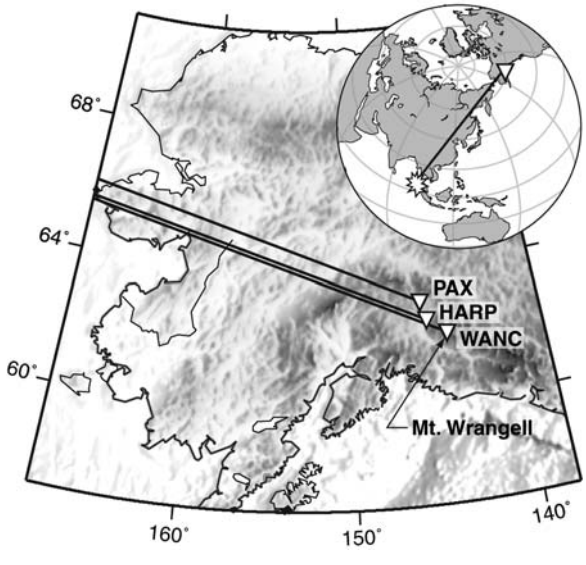

Fig. 1. Map with great circle paths from Sumatra to Mount Wrangell. Surface waves arrived at Wrangell from the west-northwest. Station WANC is at the summit of Wrangell. Three other short-period stations, including one three-component instrument (not shown), are located within 10 km of WANC. Stations PAX and HARP are nearby broadband instruments that are 115 and 72 km from WANC, respectively.

Alaska Volcano Observatory, Geophysical Institute, University of Alaska, Fairbanks, AK 99775, USA.

*To whom correspondence should be addressed. E-mail: west@gi.alaska.edu